Facile preparation and dye removal properties of Fe_3O_4@carbon nanocomposite

Di Kong[1], Yunfang Liu[1] ✉, Yangyang Li[1], Weidong Chi[1], Qigu Huang[1], Changyuan Yu[2]

[1]*Key Laboratory of Carbon Fibers and Functional Polymers of Ministry of Education, Beijing University of Chemical Technology, Beijing 100029, People's Republic of China*
[2]*College of Life Science and Technology, Beijing University of Chemical Technology, Beijing 100029, People's Republic of China*
✉ *E-mail: liuyunfang@mail.buct.edu.cn*

Published in Micro & Nano Letters; Received on 29th June 2017; Revised on 11th September 2017; Accepted on 12th October 2017

Fe_3O_4@carbon nanocomposite (Fe_3O_4@C) was continuously prepared by combining microreactor with pyrolysis reactor. The Fe_3O_4 nanoparticles homogeneously disperse in the carbon matrix with an average size of about 9.2 nm and narrow size distribution. The Fe_3O_4@C nanocomposite has a Brunauer–Emmett–Teller specific surface area of 71.9 m^2/g and total pore volume of 0.37 cm^3/g. This nanocomposite has a saturation magnetisation value of 16 emu/g and could be easily separated from water by an external magnet. With the increase of pH value or temperature, the Rhodamine B absorbing capacity of the Fe_3O_4@C nanocomposite first increases and then decreases after a certain value. The absorbing capacity at pH value 9 is about 169 mg/g when the temperature is 20°C. The above said value also exceeds 150 mg/g at pH value 3. The capacity is still higher than 120 mg/g after four regenerations. The absorbing capacity even reaches to 184 mg/g at 60°C of the absorbing temperature.

1. Introduction: Fe_3O_4-based core/shell composites as multi-functional materials have been used in many fields due to their unique properties, such as energy storage, pollution absorption, photothermal therapies and microwave absorption [1–4]. Various shell materials were used including carbon, metals, metal oxides, SiO_2 and polymer. Recently, Fe_3O_4@carbon nanocomposite (Fe_3O_4@C) has attracted great attention and is looked as a good magnetic absorption material because of its strong absorption ability and high separation efficiency [2, 5, 6]. Compared with other usual carbon nanocomposites or metal oxide nanoparticles (NPs), Fe_3O_4@C nanocomposite could combine the advantages of magnetic Fe_3O_4 and porous carbon. Many methods have been used for Fe_3O_4@C nanocomposites. One-step hydrothermal synthesis is a widely traditional one-step method for Fe_3O_4@C. This method is a time-consuming and batch-type technology, and usually suffers severe Fe_3O_4 aggregation. Multi-step methods are also widely used for Fe_3O_4@C nanocomposites. The processes usually have three main steps (preparations of Fe_3O_4, Fe_3O_4@C precursor and Fe_3O_4@C in turn). Those methods inevitably need a long preparation period and undergo some intermediate steps. As a result, severe Fe_3O_4 aggregations will form. It is well known that the properties of Fe_3O_4@C nanocomposites will be impaired by Fe_3O_4 aggregations. Fe_3O_4 is also one of the key factors that affect the properties of Fe_3O_4@C nanocomposites [2]. The classical precipitation technology was widely used for Fe_3O_4 NPs. However, some problems still need to be solved for the traditional method, such as wide size distribution and severe aggregation. Many modified co-precipitation methods have been exploited.

Micro-flow reaction as one new kind of chemical process intensification technologies has been used to prepare many materials, such as polymers, inorganic materials and nanocomposites [7–10]. The microfluidic method has many advantages for the preparation of NPs, such as high-effective mixing with strict stoichiometry, easy controllability and easy mass production without amplification effect. The obtained NPs had relatively small size and narrow size distribution. When the micro-flow reaction technology is introduced to precipitation method, some problems encountered in traditional method could be effectively resolved. Compared with Fe_3O_4 NPs from traditional method, the Fe_3O_4 NPs prepared by microfluidic method have relatively small size and narrow size distribution [2]. Spraying pyrolysis is a commonly used method for many carbonaceous materials, such as carbon nanotubes, porous carbon [11–13]. In this research, we tried to couple the micro-flow reactor and pyrolysis reactor for continuously preparing Fe_3O_4@C nanocomposite. This new one-step method could avoid some problems in multi-step methods or one-step hydrothermal method. The morphology, structure, magnetic and Rhodamine B (RhB) absorption property of this Fe_3O_4@C nanocomposite were investigated. The effects of the RhB concentrations, pH values, temperatures on the RhB absorption of the Fe_3O_4@C nanocomposite were studied.

2. Experimental section

2.1. Preparation of Fe_3O_4@C nanocomposite: The preparation process of Fe_3O_4@C nanocomposite was carried as several steps: (i) aqueous solution A ($FeCl_3$: 0.05 mol/l and $FeSO_4$: 0.025 mol/l) and aqueous solution B (NaOH: 0.2 mol/l and soluble starch: 0.125 mol/l) were prepared; (ii) both solutions were separated pumped at constant flow rate (20 ml/min) into two inlets of a micro-mixer; (iii) the reacted liquid was directly introduced through a PTFE tube ((ID: 0.5 mm, length: 1 m) into an ultrasonic spray nozzle (G40M, Siansonic Technology Ltd) and then into a pyrolysis reactor (500°C); (iv) the reactants were passed through the high-temperature region by carrier gas N_2 (1 l/min) to react; (v) the production was collected in a collector. For comparison, pure Fe_3O_4 NPs were prepared as the above said process just without soluble starch in solution B.

2.2. Adsorption and recovery experiments: The RhB molecule was used as a model compound to evaluate the adsorption property of the Fe_3O_4@C nanocomposite. The absorption process was carried in dark environment and the detail is as follows: (i) RhB solution (100 ml) with special pH value (3–11) was first prepared and the pH value was adjusted using HCl or NaOH solution (2 M); (ii) the absorbing material was added into the above solution and agitated at a constant temperature (20–70°C); (iii) after some time, the absorbing material was separated from the solution via a magnet; (iv) the solution was taken to measure the RhB concentration through a UV–Vis spectrophotometer

(554 nm), and the adsorption capacity q_t was calculated according to the following equation:

$$q_t = (C_0 - C_t)/C_a \quad (1)$$

In the above equation, C_0 is the initial RhB concentration, C_t is the residual RhB concentration after absorption and C_a is the concentration of absorption material (50 mg).

The reusability of the Fe_3O_4@C nanocomposite was performed as follows: (i) after separated from solution for one batch absorbing experiment, the Fe_3O_4@C nanocomposite was simply washed with de-ion water several times and further dried in an oven at 110°C for 12 h; (ii) the recovered Fe_3O_4@C nanocomposite was used for the next adsorption experiment.

The recovery of the Fe_3O_4@C nanocomposite was also evaluated as follows: (i) Fe_3O_4@C nanocomposite was added into de-ion water and dispersed by agitation; (ii) Fe_3O_4@C nanocomposite was separated from water by an external magnet and dried in an oven at 110°C for 12 h; (iii) the dried sample was weighed and the recovery η was calculated according to the following equation:

$$\eta = (m_0 - m)/m_0 \quad (2)$$

In the above equation, m_0 is the initial mass of the nanocomposite and m is the mass of the recovered nanocomposite.

2.2. Characterisations: The transmission electron microscopy (TEM, FEI, Tecnai-G20) and X-ray diffraction (XRD, Rigaku, D/Max2500) were used to observe the microstructures and crystal structures of the samples, respectively. The surface and magnetic property were analysed by infrared spectrum analyser (IR, TNZ1-5700) and vibrating sample magnetometer (EG & GVSM Model 155). The X-ray photoelectron spectra (XPS, Thermo Fisher Scientific, Escalab250) was used to observe the surface chemical states of the materials. The nitrogen adsorption and desorption isotherm was measured at −196°C on volumetric analyser (NOVA4200e). The Brunauer–Emmett–Teller method and density functional theory (DFT) were used to calculate the surface area and pore size distribution, respectively.

3. Results and discussions: The TEM image of the Fe_3O_4@C nanocomposite and the size-distribution histogram of the corresponding Fe_3O_4 NPs are shown in Fig. 1. The Fe_3O_4 NPs are homogeneously dispersed in the carbon matrix without obvious big NP aggregation. The Fe_3O_4@C nanocomposite has a sheet-like structure. This nanocomposite is different from that with spherical structure from other methods [3, 4]. It is possibly due to the water environment with low carbon concentration and short reaction time. However, the real reason still needs to be carefully studied. The very weak image contrast of the carbon shell shows its amorphous structure. More than 260 Fe_3O_4 NPs in the nanocomposite were measured to get the size distribution histogram, as shown in Fig. 1*c*. The Fe_3O_4 NPs formed in the microreactor system have an average size of about 9.2 nm with narrow size distribution.

Fig. 2*a* shows the XRD patterns of the Fe_3O_4 NPs and Fe_3O_4@C nanocomposite. The pure Fe_3O_4 NPs display a standard diffraction pattern of Fe_3O_4 material (JCPDS Card No. 03-0863). No obvious carbon diffraction peak was found in the XRD pattern of the Fe_3O_4@C nanocomposite, which indicates the amorphous carbon structure. This result coincides with the TEM observation. Fig. 2*b* is the IR spectra of the samples. The peak at about 570 cm^{-1} is contributed to the Fe–O stretching vibration [6]. The peaks at about 1600 and 1696 cm^{-1} are assigned to C=C and C=O vibrations [6]. The XPS spectrum of the Fe_3O_4@C nanocomposite in Fig. 2*c* clearly exhibits the existence of the iron, carbon and oxygen elements. The insert amplified spectrum displays the

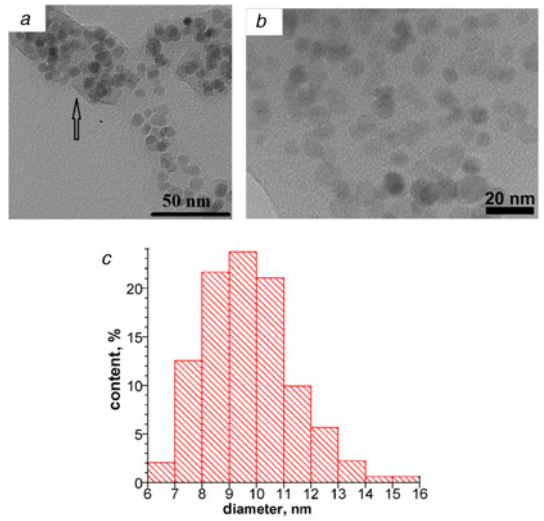

Fig. 1 *TEM image and size-distribution histogram*
a, *b* TEM image of Fe_3O_4@C nanocomposite
c Size-distribution histogram of Fe_3O_4 NPs

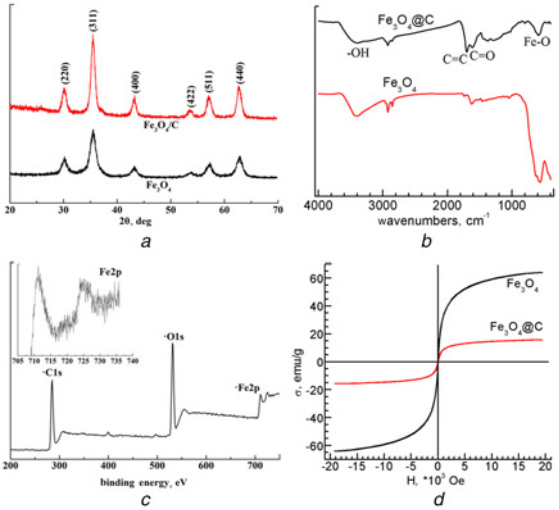

Fig. 2 *XRD, Fourier-transform infrared spectroscopy (FTIR), XPS and magnetisation hysteresis loops of Fe_3O_4 and Fe_3O_4@C nanocomposite*
a XRD
b FTIR
c XPS
d Magnetisation hysteresis loops\

existence of Fe^{3+} and Fe^{2+}. As it can be seen from the magnetisation hysteresis loops in Fig. 2*d*, the saturation magnetisation values of the Fe_3O_4 NPs and Fe_3O_4@C nanocomposite have 56.1 and 16 emu/g, respectively. The Fe_3O_4@C nanocomposite could be easily separated from water by a magnet. Its recovery could reach to 99.1% that exhibits good magnetic recovery ability.

The N_2 adsorption–desorption isotherm of the Fe_3O_4@C nanocomposite is presented in Fig. 3*a*. It clearly shows only a few micropores in this nanocomposite. The obvious capillary condensation phenomenon at high relative pressure in N_2 adsorption–desorption isotherm demonstrates the existence of the mesopore structure. The specific surface and pore volume of the Fe_3O_4@C nanocomposite are 71.9 m^2/g and 0.37 cm^3/g, respectively. Its pore distribution curve in Fig. 3*b* calculated by DFT also shows the mesopore structure in the nanocomposite. The calculated average pore size is about 20.4 nm. The mesopore structure is in favour of dye absorption.

Fig. 4 shows the RhB isothermal absorption curves of the Fe_3O_4@C nanocomposite at different initial RhB concentrations

doi: 10.1049/mnl.2017.0478

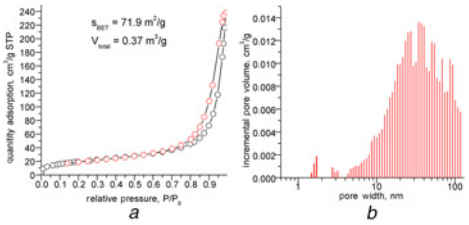

Fig. 3 *Absorption–desorption isotherm and pore size distribution of Fe_3O_4@C*
a Absorption–desorption isotherm
b Pore size distribution

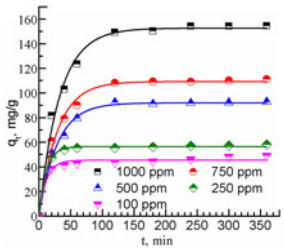

Fig. 4 *RhB isothermal absorption curves of Fe_3O_4@C nanocomposite (at 20°C)*

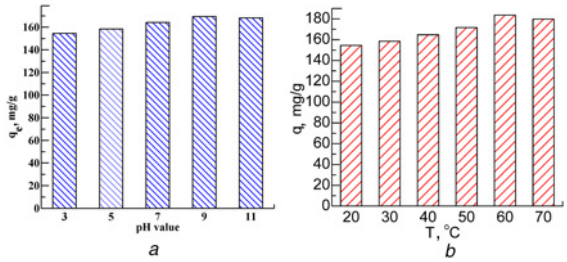

Fig. 5 *Effect of pH and temperature on absorption capacity of Fe_3O_4@C*
a Effect of pH
b Effect of temperature

(20°C, pH value 3). The absorption capacities approach to the saturation values in 120 min. At 1000 ppm of RhB concentration, the saturation absorption capacity is about 155 mg/g. The effects of pH value and temperature on the dye absorption are further investigated as shown in Fig. 5. When the temperature is kept at 20°C, the absorption capacity slightly increases with the increase of pH value and reaches a maximum value at about 9 (about 169 mg/g). The smallest that value in our researched pH range is also as high as about 155 mg/g (pH value 3). Different pH values in solution will lead to different surface ionic charges and textural properties of the adsorbent and adsorbate that determine the adsorption behaviour [14–17]. At relatively low pH value, the surface state of Fe_3O_4@C nanocomposite is positive and the RhB are of cationic and monomeric molecular form. The RhB cation has a relatively weak interaction with the nanocomposite, but it could easily enter into the pore structure of the nanocomposite. Increasing pH value will lead to the increase of the charges on the Fe_3O_4@C nanocomposite that will strengthen the interaction. However, at high pH value, the formed RhB aggregations (dimers) will outstandingly produce strong steric hindrance for RhB into the pore structure. Actually, the ion concentrations (Cl^-, Na^+ and others) in the dye solution will have great effect on the absorption. That is needed for further investigation. When the pH value is kept at 3, the absorption capacity of the Fe_3O_4@C nanocomposite increases with the increase of temperature and reaches a maximum value at about

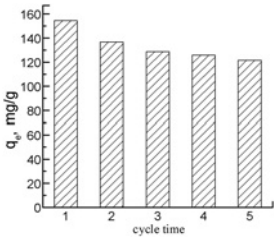

Fig. 6 *Reusability of Fe_3O_4@C nanocomposite*

60°C (about 184 mg/g). The capacity decreases to 179.8 mg/g at 70°C. The diffusion is an endothermic process and high temperature is in favour of the action of dye molecule [14–18]. So the absorption capacity increases with raising the temperature. However, the interaction of RhB molecule with the nanocomposite is easily broken at a relatively high temperature, which leads to the decrease of the absorption capacity. The reusability of the nanocomposite was further valuated at a constant condition (20°C and pH value 3). As shown in Fig. 6, the saturation absorption capacity just slightly decreases to 122 mg/g after four-time regeneration from 155 mg/g. In the regeneration experiment, the used Fe_3O_4@C nanocomposite was just simply washed several times with di-ion water. The simple purge process cannot remove all the absorbed RhB molecules. The residual RhB molecules inevitably affect the next absorption. It could be deduced that a higher capacity could be kept if a better regeneration method is adopted.

4. Conclusion: In conclusion, we successfully developed a facile continuous-flow synthesis method for Fe_3O_4@C nanocomposite by combining microfluidic synthesis with spray pyrolysis. The Fe_3O_4@C nanocomposite is easily withdrawn from water by a magnet, whose recovery is about 99.1%. The RhB saturation absorption capacity at relatively optimal condition of this Fe_3O_4@C nanocomposite exceeds 184 mg/g. In our researched conditions, the smallest absorbing capacity is also 155 mg/g at 30°C and pH value 3. The capacity after four-time regeneration is still as high as 122 mg/g at this condition, which shows an excellent renewability.

5. Acknowledgments: This work was supported by the Fundamental Research Funds for the Central Universities of China (grant no. JD1406), and the National Natural Science Foundation of China (grant nos. 21174011 and U1462102).

6 References

[1] Zhu Y., Bai Y.J., Han F.D., *ET AL.*: 'One-step preparation of six-armed Fe_3O_4 dendrites with carbon coating applicable for anode material of lithium-ion battery', *Mater. Lett.*, 2011, **65**, (19–20), pp. 3157–3159
[2] Liu Y.F., Li Y.Y., Zhao X., *ET AL.*: 'Effect of magnetite nanoparticles on dye absorption properties of magnetite@carbon composites', *B. Mater. Sci.*, 2017, **40**, (2), pp. 367–373
[3] Ren J.F., Shen S., Pang Z.Q., *ET AL.*: 'Facile synthesis of superparamagnetic Fe_3O_4@Au nanoparticles for photothermal destruction of cancer cells', *Chem. Commun.*, 2011, **47**, (42), pp. 11692–11694
[4] Qiao M.T., Lei X.F., Ma Y., *ET AL.*: 'Dependency of tunable microwave absorption performance on morphology-controlled hierarchical shells for core-shell Fe_3O_4@MnO_2 composite microspheres', *Chem. Eng. J.*, 2016, **304**, (15), pp. 552–562
[5] Zhao L.Q., Chang X.L., Liao R., *ET AL.*: 'Facile hydrothermal preparation of S-doped Fe_3O_4@C nanoparticles for Cu^{2+} removal', *Mater. Lett.*, 2014, **135**, (15), pp. 154–157
[6] Zhang Y.X., Xu S.C., Luo Y.Y., *ET AL.*: 'Synthesis of mesoporous carbon capsules encapsulated with magnetite nanoparticles and their application in wastewater treatment', *J. Mater. Chem.*, 2011, **21**, (11), pp. 664–671
[7] Jahnisch K., Hessel V., Lowe H., *ET AL.*: 'Chemistry in microstructured reactors', *Chem. Int. Ed. Engl.*, 2004, **43**, (4), pp. 406–446

[8] Song Y.J., Hormes J., Kumar C.S.S.R.: 'Microfluidic synthesis of nanomaterials', *Small*, 2008, **4**, (6), pp. 698–711
[9] Zhao C.X., He L.Z., Qiao S.Z., *ET AL.*: 'Nanoparticle synthesis in microreactors', *Chem. Eng. Sci.*, 2011, **66**, (7), pp. 463–479
[10] Yao X.J., Zhang Y., Du L.Y., *ET AL.*: 'Review of the applications of microreactors', *Renew. Sustain. Energy Rev.*, 2015, **47**, pp. 519–539
[11] Pan Y., Liu Y.F., Chi W.D., *ET AL.*: 'Inner-diameter enlargement of multi-walled carbon nanotubes by adding HBO_3 in catalyst', *Mater. Lett.*, 2011, **65**, (23–24), pp. 362–364
[12] Annu A., Bhattacharya B., Singh P.K., *ET AL.*: 'Carbon nanotube using spray pyrolysis: recent scenario', *J. Alloy Compd.*, 2017, **691**, pp. 970–982
[13] Skrabalak S.E., Suslick K.S.: 'Porous carbon powders prepared by ultrasonic spray pyrolysis', *J. Am. Chem. Soc.*, 2006, **128**, (39), pp. 12642–12643
[14] Zhang Z.Y., Kong J.L.: 'Novel magnetic Fe_3O_4@C nanoparticles as adsorbents for removal of organic dyes from aqueous solution', *J. Hazard. Mater.*, 2011, **193**, (5), pp. 325–329
[15] Peng L., Qin P.F., Lei M., *ET AL.*: 'Modifying Fe_3O_4 nanoparticles with humic acid for removal of rhodamine B in water', *J. Hazard. Mater.*, 2012, **209–210**, (1), pp. 193–198
[16] Tripathi P.K., Liu M.X., Gan L.H., *ET AL.*: 'High surface area ordered mesoporous carbon for high-level removal of rhodamine B', *J. Mater. Sci.*, 2013, **48**, (22), pp. 8003–8013
[17] Gad H.M.H., El-Sayed A.A.: 'Activated carbon from agricultural by-products for the removal of Rhodamine-B from aqueous solution', *J. Hazard. Mater.*, 2009, **168**, (2–3), pp. 1070–1081
[18] Bujdak J., Iyi N.: 'Molecular aggregation of Rhodamine dyes in dispersions of layered silicates: influence of dye molecular structure and silicate properties', *J. Phys. Chem. B*, 2006, **110**, (5), pp. 2180–2186

doi: 10.1049/mnl.2017.0478